Coupled Macroscopic Modelling of Electric Vehicle Traffic and Energy Flows for Electromobility Control

Mladen Čičić, Carlos Canudas de Wit

Coupled Macroscopic Modelling of Electric Vehicle Traffic and Energy Flows for Electromobility Control

Mladen Čičić and Carlos Canudas-de-Wit

***Abstract*— The simultaneous proliferation of electric vehicles and intermittent renewable energy sources promises to expedite decarbonization of two sectors with highest emissions. However, both these developments threaten to endanger power system stability, which may hinder their widespread adoption. To tackle these challenges, there is a need for joint modelling of electric vehicle traffic flows, together with their battery dynamics. We propose a macroscopic electromobility model, augmenting the LWR model, describing the traffic dynamics, with an inhomogeneous advection equation, describing the evolution of vehicles' State of Charge (SoC). The Riemann problem for the joint model is solved for the case of triangular fundamental diagram, and the solutions are used to formulate a Godunov-like scheme for model discretization. Additionally, we propose an advection-based charging station model, discretize it, and link it with the rest of the traffic and SoC model. We demonstrate the capabilities and use of the full coupled model by proposing a pedagogic example where a simple control law regulates the average SoC of all vehicles on a ring road by controlling the traffic flow entering the charging station.**

I. Introduction

The emergent coupling between the transportation and power systems, brought about by the rise of electric vehicles (EVs), will have far-reaching consequences for both sectors [1]. From the mobility side, the range constraints, need for charging, and drivetrain specificities need to be taken into account when making routing decisions and considering driving strategies for EVs [2]. Furthermore, dynamic charging price policies might affect the flows of EVs, potentially providing a way to influence mobility patterns [3]. From the power system side, the EVs will be a significant contributor to the overall power demand due to their charging needs [4], but could also be used to provide power system flexibility (ability to react to changing conditions by storing energy or changing power supply or demand). Recently, there has been much interest in using EVs and their batteries to provide ancillary services [5], [6], by shaping their aggregated power demand, or even providing Vehicle-to-Grid (V2G) power and energy storage via bidirectional charging stations, which is likely to be crucial for renewable energy integration [7].

For all these reasons, there is a need to consider both the transportation system and the power system holistically. For example, [3] considers static EV traffic assignment using power and congestion pricing, taking into account the full coupled transportation-power system. In [8], the authors use a dynamic traffic assignment model connected with the power grid to study equilibrium flow patterns. These works, and references therein, approach the problem at the scale of full networks. Other works focus on individual EVs, modelling their power consumption based on propulsion and braking forces [9], or driving behaviour and ambient factors [10]. However, to the authors' best knowledge, this modelling problem was not approached from the macroscopic traffic modelling perspective, describing both energy and traffic flows on a road, which this work seeks to address.

Many recently introduced macroscopic traffic models belong to the GSOM family [11] (Generic second order modelling). These models augment the base traffic dynamics, described by the Lighthill-Whitham-Richards (LWR) model [12], to include some additional property (e.g. aggressiveness, portion of connected and automated vehicles, etc.) which is conserved and advected (transported) along the trajectories of individual vehicles, as proposed in [13], and used to specify the driver behaviour. We propose that a similar approach can be applied to advected properties that are not conserved, such as the State of Charge (SoC) of EVs.

The main contribution of this work is in proposing a coupled macroscopic model for traffic and energy flows of EVs. The traffic flow dynamics, described by the LWR model, are augmented with flows of energy, carried by vehicles SoC. While vehicles are driving on the road, energy contained in their batteries is advected, and dissipated according to the battery discharge model. While charging, the vehicles' SoC evolution is described by the charging station model, providing a convenient interface for interconnection with the power system. The model is similar to the one proposed in [5], but it models EVs charging at individual charging stations, and allows for different charging rates at different SoC, instead of relying on splitting the EVs into charging, idle, and discharging categories. All model components are discretized using a Godunov-like scheme based on the presented Riemann problem solution for the triangular flux function case, and charging stations are interconnected with the road dynamics via on- and off-ramps. Finally, a control law based on the simplified approximate prediction model is used to regulate the average SoC of all vehicles on the road by controlling flows to the charging station. This model will serve as a basis for more sophisticated models to be envisioned in the future, that would be used to study the interplay between the power grid operators and the EVs.

The rest of this paper is organized as follows. In Section II, we introduce the proposed coupled traffic, energy, and charging (CTEC) model, and then in Section III discuss its discretization and coupling via ramp flows. Next, in

Mladen Čičić and Carlos Canudas-de-Wit are with Univ. Grenoble Alpes, CNRS, Inria, Grenoble INP, GIPSA-lab, 38000 Grenoble, France (e-mail: {cicic.mladen, carlos.canudas-de-wit}@gipsa-lab.fr)

Section IV, we design control laws for regulating the SoC of the vehicles on a road, which are then test in simulations in Section V. Finally, in Section VI, we summarize the results and outline some future work directions.

II. CTEC MODEL

In this section, we present the different components of the CTEC model: EV traffic, battery discharging, and charging stations dynamics.

A. Traffic model

We use the LWR model [12] to model the traffic flow dynamics,

$$\frac{\partial \rho}{\partial t} + \frac{\partial Q(\rho)}{\partial x} = 0, \tag{1}$$

where $\rho(x,t)$ denotes the traffic density at position x and time t, and $Q(\rho)$ is the flux function (also known as fundamental diagram) that describes the dependence of traffic flow on the traffic density. The average vehicle flow speed $\mathcal{V}(\rho)$ also directly depends on the traffic density, since $Q(\rho) = \mathcal{V}(\rho)\rho$. In this work, we use the triangular fundamental diagram,

$$Q(\rho) = \min\{V\rho, W(P-\rho)\} \tag{2}$$

V is the free-flow speed, W the congestion wave speed, and P the jam density, yielding critical density $\sigma = \frac{WP}{V+W}$, and

$$\mathcal{V}(\rho) = \begin{cases} V, & \rho \le \sigma, \\ W\left(\frac{P}{\rho} - 1\right), & \rho > \sigma. \end{cases}$$

B. Energy model

The discharge rate of EV batteries depends on a plethora of influences [10], but the main contributor is naturally their motion. We denote the SoC of vehicle ξ as $\varepsilon_\xi(t) \in [0,1]$, and approximate its discharge during driving as

$$\dot{\varepsilon}_\xi(t) = \mathcal{D}_\xi(x_\xi(t)), \tag{3}$$

where $x_\xi(t)$ is the vehicle's trajectory. Typically, the rate of discharge is assumed to depend on vehicle speed $\dot{x}_\xi(t)$ and acceleration $\ddot{x}_\xi(t)$.

We can instead study the macroscopic SoC of all vehicles at different positions on the road $\varepsilon(x,t) \in [0,1]$, modelling the evolution of $\varepsilon(x,t)$ as an inhomogeneous linear transport PDE with speed varying in space and time as a function of traffic density,

$$\frac{\partial \varepsilon}{\partial t} + \mathcal{V}(\rho)\frac{\partial \varepsilon}{\partial x} = \mathcal{D}(\rho) \tag{4}$$

where $\mathcal{D}(\rho(x,t))$ models the battery discharge dynamics depending on the traffic conditions, analogous to $\mathcal{D}_\xi(x_\xi(t))$. Here we assume that ε has no direct impact on the traffic flow, by e.g., having some vehicles run out of charge. Since the traffic dynamics are such that the trajectories of the vehicles never intersect, using the method of characteristics, we may confirm that the SoC along trajectories of the vehicles $\dot{x}_\xi(t) = \mathcal{V}(\rho(x_\xi(t),t))$ evolves as $\dot{\varepsilon}_\xi(t) = \mathcal{D}(\rho(x_\xi(t),t))$, consistently with (3). Equivalently, (4) can be written in terms of energy density $\rho\varepsilon$ as

$$\frac{\partial \rho\varepsilon}{\partial t} + \frac{\partial(\mathcal{V}(\rho)\rho\varepsilon)}{\partial x} = \rho\mathcal{D}(\rho), \tag{5}$$

which can be verified by expanding the left side and substituting (1) and (4). Energy density is an important concept since it is a conserved quantity, apart from the dissipation term $\rho\mathcal{D}(\rho)$, allowing us to apply a Godunov-like scheme to numerically solve (5) coupled with (1).

The simplest way to model battery discharge rate is by assuming it is linearly proportional to vehicle speed, yielding $\mathcal{D}_\xi(x_\xi(t)) = D_1\dot{x}_\xi(t)$ and $\mathcal{D}(\rho) = D_1\mathcal{V}(\rho)$, $D_1 < 0$, in which case the spent energy depends only on the distance travelled,

$$\varepsilon_\xi(t_2) - \varepsilon_\xi(t_1) = \int_{t_1}^{t_2} \mathcal{D}_\xi(x_\xi(t))\mathrm{d}t = D_1(x_\xi(t_2) - x_\xi(t_1))$$

if $\dot{x}_\xi(t) \ge 0$ for all t, and the range of the EV is $-\frac{1}{D_1}$. A special form of the problem is for $\mathcal{D}(\rho) = 0$, in which case we model the advection of some quantity ε by vehicles in traffic, and the model belongs to the GSOM family [11].

C. Charging stations model

In order to model the SoC dynamics of charging vehicles, some simplifying assumptions need to be made about the charging speed. We denote the charging rate of vehicle ξ, within charging station ζ and with current SoC $\varepsilon_\xi(t)$, as $c_\zeta(\varepsilon_\xi, t)$, yielding $\dot{\varepsilon}_\xi = c_\zeta(\varepsilon_\xi(t), t)$. The charging dynamics of an ensemble of charging vehicles can then be modelled macroscopically as an advection equation

$$\frac{\partial \eta_\zeta}{\partial t} + \frac{\partial(c_\zeta(\varepsilon,t)\eta_\zeta)}{\partial \varepsilon} = 0, \tag{6}$$

where $\eta_\zeta(\varepsilon,t)$ denotes the number of vehicles in charging station ζ with SoC ε at time t, and we need $c_\zeta(0,t) \ge 0$ and $c_\zeta(1,t) \le 0$ to ensure the SoC remains within $[0,1]$. Note that the charging rate $c_\zeta(\varepsilon,t)$ for each (ε,t) may either be positive, modelling charging the batteries of the EV, negative, modelling V2G energy flow, or zero.

The coupling between the charging stations and the road is done through on- and off-ramp dynamics. These flows are not explicitly defined in the CTEC model, where they would enter as additional source terms, but are instead defined in the discretized version of the model presented in further text.

III. CTEC MODEL DISCRETIZATION

In order to enable numerical evaluation of the CTEC model presented in the previous Section, we now discuss its discretization in space and time. First, the Riemann problem for traffic and energy density is solved, then its solution is used to formulate a Godunov-like discretization scheme, and finally, the road and the charging stations are connected by describing the ramp dynamics.

A. Riemann problem for traffic and energy density

Riemann problems, i.e., PDE initial value problems given piecewise-constant initial conditions with a single discontinuity, arise naturally in Godunov-like schemes used for PDE discretization, since they describe what happens at the boundary between two cells. The Riemann problem for (1) and (4) or (5),

$$\rho(x,0) = \begin{cases} \rho_-, & x < 0, \\ \rho_+, & x > 0, \end{cases} \quad \varepsilon(x,0) = \begin{cases} \varepsilon_-, & x < 0, \\ \varepsilon_+, & x > 0, \end{cases}$$

can be split into two parts, determining $\rho(x,t)$ first by solving the Riemann problem for (1), and then using this solution in the Riemann problem for (5), since the coupling between ρ and ε is only unidirectional. Due to the assumption that the SoC everywhere is such that it does not affect the motion of the vehicle, the evolution of ρ does not depend on ε. The full Riemann problem with triangular flux function $Q(\rho)$ (2), can be solved explicitly,

$$\rho(x,t)=\begin{cases}\rho_-, & x<\lambda_- t,\\ \sigma, & \lambda_- t<x<\lambda_+ t,\\ \rho_+, & x>\lambda_+ t,\end{cases} \quad (7)$$

$$\varepsilon(x,t)=\begin{cases}\varepsilon_-+d_- t, & x<\lambda_- t,\\ \varepsilon_-+d_-\frac{x-v_+t}{\lambda_- -v_+}+d_+\frac{\lambda_- t-x}{\lambda_- -v_+}, & \lambda_- t<x<v_+ t,\\ \varepsilon_++d_+ t, & x>v_+ t,\end{cases} \quad (8)$$

where we write $v_\pm=\mathcal{V}(\rho_\pm)$, $d_\pm=\mathcal{D}(\rho_\pm)$, and λ_- and λ_+ are the propagation speeds of the upstream- and downstream-most wavefront originating from $x=0$ at $t=0$, respectively,

$$\lambda_-=\begin{cases}\frac{v_+\rho_+-v_-\rho_-}{\rho_+-\rho_-}, & \rho_-\le\sigma,\\ -W, & \rho_->\sigma,\end{cases} \quad (9)$$

$$\lambda_+=\begin{cases}\frac{v_+\rho_+-v_-\rho_-}{\rho_+-\rho_-}, & \rho_+>\sigma,\\ V, & \rho_+\le\sigma.\end{cases} \quad (10)$$

An example Riemann problem solution is shown in Fig. 1. Unless $\rho_->\sigma$ and $\rho_+<\sigma$, these two wavefronts coincide, and $\rho(x,t)$ has only one discontinuity in x, $t\ge 0$, except in the degenerate case when $\rho_-=\rho_+$. The energy density $\rho(x,t)\varepsilon(x,t)$ can be written jointly, multiplying (7) and (8),

$$\rho(x,t)\varepsilon(x,t)=\begin{cases}\rho_-(\varepsilon_-+d_- t), & x<\lambda_- t,\\ \sigma\left(\varepsilon_-+\frac{d_-(x-v_+t)+d_+(\lambda_- t-x)}{\lambda_- -v_+}\right), & x\in(\lambda_- t,\lambda_+ t),\\ \rho_+\left(\varepsilon_-+\frac{d_-(x-v_+t)+d_+(\lambda_- t-x)}{\lambda_- -v_+}\right), & x\in(\lambda_+ t,v_+ t),\\ \rho_+(\varepsilon_++d_+ t), & x>\lambda_+ t.\end{cases} \quad (11)$$

B. Godunov scheme for traffic density

Discretization of the LWR model (1) using Godunov scheme yields the Cell Transmission Model [14], [15]. Splitting the road into N_x cells, we denote by ρ_i^k the average traffic density in cell i at time step k, and it is updated as

$$\rho_{i+1}^k=\rho_i^k+\frac{T}{L}\left(q_{i-}^k-q_{i+}^k\right) \quad (12)$$

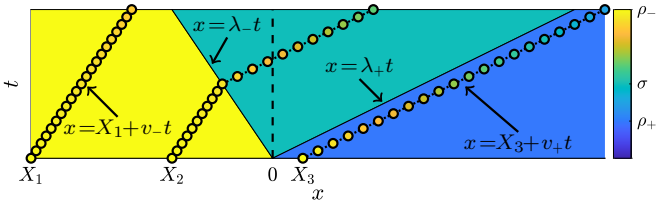

Fig. 1: Riemann problem solution with colour-coded traffic density (warmer is denser) shown in the background , and SoC evolution along three example vehicle trajectories shown by the colour of the circles (warmer is higher). Once vehicles cross the wavefront $x=\lambda_- t$ and leave the congestion (ρ_-, yellow), they proceed at higher speed, incurring faster reduction of SoC.

where $T\le\frac{L}{V}$ ensures numeric stability, q_{i-}^k is the traffic flow at the upstream boundary of cell i (from cell $i-1$ to cell i), and q_{i+}^k at its downstream boundary (from i to $i+1$),

$$q_{i+}^k=\min\left\{V\overline{\rho}_i^k, W(P-\underline{\rho}_{i+1}^k)\right\}=q_{i+1-}^k,$$

denoting $\underline{\rho}_i^k=\max\{\rho_i^k,\sigma\}$, and $\overline{\rho}_i^k=\min\{\rho_i^k,\sigma\}$.

It is also possible to rewrite the traffic density update (12) into a form that more directly reflects the solutions to the Riemann problem (7),

$$\rho_{i+1}^k=\rho_i^k+\frac{T}{L}\left(\underline{\lambda}_{i_-^+}^k(\overline{\rho}_{i-1}^k-\rho_i^k)-\overline{\lambda}_{i_+^-}^k(\underline{\rho}_{i+1}^k-\rho_i^k)\right),$$

denoting $\underline{\lambda}_{i_-^+}^k=\max\{0,\lambda_{i_-^+}^k\}$, and $\overline{\lambda}_{i_+^-}^k=\min\{0,\lambda_{i_+^-}^k\}$. Wavefront speeds $\lambda_{i_*^\circ}^k$ arise from the solutions to the Riemann problems at the boundaries of cell i at time k, with $*\in\{-,+\}$ denoting whether we consider the upstream ($-$) or downstream ($+$) boundary, and $\circ\in\{-,+\}$ denotes whether we are looking for the upstream-most ($-$), or downstream-most ($+$) wavefront. If $\circ=-$, $\lambda_{i_*^-}^k$ is given by λ_- in (9), and if $\circ=+$, $\lambda_{i_*^+}^k$ is given by λ_+ in (10). In both cases, $\rho_\pm$ and $v_\pm$ in expressions (9) and (10) are given by $\rho_-=\rho_{i-1}^k$, $\rho_+=\rho_i^k$, $v_-=v_{i-1}^k$, $v_+=v_i^k$, if $*=-$, or by $\rho_-=\rho_i^k$, $\rho_+=\rho_{i+1}^k$, $v_-=v_i^k$, $v_+=v_{i+1}^k$, if $*=+$. Note that for convenience of notation, in this work we denote $v_i^k=\mathcal{V}(\rho_i^k)$ which may not reflect the actual current average speed of vehicles in cell i in case the cell lies on the boundary between congestion and free flow. A similar form will be employed when formulating the energy density update.

C. Godunov-like scheme for energy density

We describe the evolution of the SoC $\varepsilon(x,t)$ indirectly, through finding the updates to the energy density $\rho(x,y)\varepsilon(x,t)$. To simplify the expressions, we adopt $T\le\frac{L}{V+W}$, ensuring that wavefronts originating from cell up- and downstream boundary do not collide, so each vehicle encounters at most one wavefront. We denote by ε_i^k the average SoC in cell i at time step k. Based on (11), the energy density update can be expressed as

$$\begin{aligned}L\rho_i^{k+1}\varepsilon_i^{k+1}=&\rho_{i-1}^k I_{i,1}(0,\underline{\lambda}_{i_-^-}^k T)+\underline{\rho}_i^k I_{i,2}(\underline{\lambda}_{i_-^-}^k T, v_i^k T)\\ &+\rho_i^k I_{i,3}(v_i^k T, L+\overline{\lambda}_{i_+^-}^k T)+\underline{\rho}_{i+1}^k I_{i,4}(\overline{\lambda}_{i_+^-}^k T,0),\end{aligned} \quad (13)$$

where $I_{i,j}, j=1,2,3,4$ are given as integrals of parts of (8),

$$\begin{aligned}I_{i,1}(x_1,x_2)=&(\varepsilon_{i-1}^k+d_{i-1}^k T)(x_2-x_1),\\ I_{i,2}(x_1,x_2)=&\left(\varepsilon_{i-1}^k+\frac{d_i^k\lambda_{i_-^-}^k-d_{i-1}^k v_i^k}{\lambda_{i_-^-}^k-v_i^k}T\right)(x_2-x_1)\\ &+\frac{d_{i-1}^k-d_i^k}{\lambda_{i_-^-}^k-v_i^k}\frac{x_2^2-x_1^2}{2},\\ I_{i,3}(x_1,x_2)=&(\varepsilon_i^k+d_i^k T)(x_2-x_1),\\ I_{i,4}(x_1,x_2)=&\left(\varepsilon_i^k+\frac{d_{i+1}^k\lambda_{i_+^-}^k-d_i^k v_{i+1}^k}{\lambda_{i_+^-}^k-v_{i+1}^k}T\right)(x_2-x_1)\\ &+\frac{d_i^k-d_{i+1}^k}{\lambda_{i_+^-}^k-v_{i+1}^k}\frac{x_2^2-x_1^2}{2},\end{aligned}$$

and $d_i^k = \mathcal{D}(\rho_i^k)$. This Godunov-like scheme simplifies to

$$\rho_i^{k+1}\varepsilon_i^{k+1} = \rho_i^k\left(\varepsilon_i^k + d_i^k T\right) + \frac{T}{L}\left(\phi_{i-}^k - \phi_{i+}^k\right),$$

with ϕ_{i-}^k and ϕ_{i+}^k given by

$$\begin{aligned}\phi_{i-}^k =& \underline{\tilde{\lambda}}_{i-}^k \tilde{\rho}_{i-}^k (\tilde{\varepsilon}_{i-}^k + \tilde{d}_{i-}^k T) + \left(v_i^k - \underline{\tilde{\lambda}}_{i-}^k\right)\underline{\rho}_i^k \tilde{\varepsilon}_{i-}^k \\ &+ \frac{T}{2}\frac{(\underline{\tilde{\lambda}}_{i-}^k - v_i^k)\underline{\rho}_i^k\left(d_i^k\left(\underline{\tilde{\lambda}}_{i-}^k - 2\tilde{\lambda}_{i-}^k + v_i^k\right) + \tilde{d}_{i-}^k\left(v_i^k - \underline{\tilde{\lambda}}_{i-}^k\right)\right)}{\tilde{\lambda}_{i-}^k - v_i^k},\end{aligned} \tag{14}$$

$$\begin{aligned}\phi_{i+}^k =& (v_i^k - \overline{\tilde{\lambda}}_{i+}^k)\rho_i^k(\varepsilon_i^k + d_i^k T) + \overline{\tilde{\lambda}}_{i+}^k \underline{\tilde{\rho}}_{i+}^k \varepsilon_i^k \\ &+ \frac{T}{2}\frac{\overline{\tilde{\lambda}}_{i+}^k \underline{\tilde{\rho}}_{i+}^k\left(d_i^k\left(\overline{\tilde{\lambda}}_{i+}^k - 2\tilde{v}_{i+}^k\right) + \tilde{d}_{i+}^k\left(2\tilde{\lambda}_{i+}^k - \overline{\tilde{\lambda}}_{i+}^k\right)\right)}{\tilde{\lambda}_{i+}^k - \tilde{v}_{i+}^k}.\end{aligned} \tag{15}$$

Here, $\tilde{\rho}_{i-}^k = \rho_{i-1}^k$, $\tilde{\rho}_{i+}^k = \rho_{i+1}^k$, $\tilde{\varepsilon}_{i-}^k = \varepsilon_{i-1}^k$, $\tilde{\varepsilon}_{i+}^k = \varepsilon_{i+1}^k$, $\tilde{v}_{i\pm}^k = \mathcal{V}(\tilde{\rho}_{i\pm}^k)$, $\tilde{d}_{i\pm}^k = \mathcal{D}(\tilde{\rho}_{i\pm}^k)$, $\tilde{\lambda}_{i-}^k$ is given by (9) with $\rho_- = \tilde{\rho}_{i-}^k$, $\rho_+ = \rho_i^k$, and $\tilde{\lambda}_{i_+^-}^k$ is given by (9) with $\rho_- = \rho_i^k$, $\rho_+ = \tilde{\rho}_{i+}^k$. Flows of traffic and energy between cells are illustrated in Fig. 2.

D. Charging stations discretization and ramp flows

Assuming the amplitude of the charging rate is bounded by some maximum rate C, $|c(\varepsilon,t)| \le C$, (6) can be discretized by dividing ε into N_ε discrete SoC levels, with discretization step S and $T \le \frac{S}{C}$, to ensure numeric stability. The evolution of the number of vehicles with discrete SoC j present at charging station ζ is then

$$\eta_{\zeta,j}^{k+1} = \eta_{\zeta,j}^k + \frac{T}{S}\left(\underline{c}_{\zeta,j-1}^k \eta_{\zeta,j-1}^k - \left|c_{\zeta,j}^k\right|\eta_{\zeta,j}^k - \overline{c}_{\zeta,j+1}^k \eta_{\zeta,j+1}^k\right), \tag{16}$$

where $\underline{c}_{\zeta,j}^k = \max\{0, c_{\zeta,j}^k\}$, $\overline{c}_{\zeta,j}^k = \min\{0, c_{\zeta,j}^k\}$, $c_{\zeta,1}^k \ge 0$, and $c_{\zeta,N_\varepsilon}^k \le 0$. Each group of vehicles $\eta_{\zeta,j}^k$ corresponds to SoC $\varepsilon = (j-1)S$, with $\eta_{\zeta,1}^k$ having SoC $\varepsilon = 0$ and $\eta_{\zeta,N_\varepsilon}^k$ SoC $\varepsilon = 1$.

Finally, the discretized CTEC model is completed by defining the interconnections between the dynamics of the road (12), (13) and the charging stations (16). A depiction of a ring-road with one charging station and one pair of on- and off-ramps is shown in Fig. 3. The road dynamics are augmented by flows from and to the charging stations or on-ramps $r_{\text{on},i}^k$, and to the charging stations or off-ramps $r_{\text{off},i}^k$,

$$\rho_i^{k+1} = \rho_i^k + \frac{T}{L}\left(q_{i-}^k - q_{i+}^k\right), \tag{17}$$

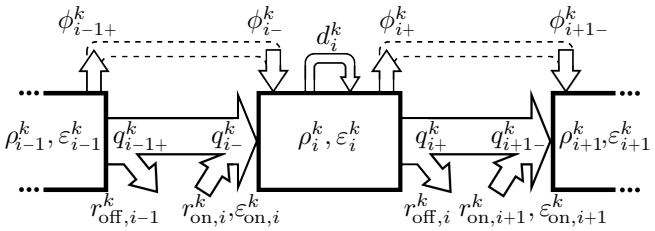

Fig. 2: Illustration of traffic and energy flows. Note that ϕ_{i-}^k and ϕ_{i+}^k do not strictly represent flows of energy over the cell boundaries, but rather the contributions of the solutions to the Riemann problem at the upstream and downstream boundary of cell i, respectively. The flows to and from on- and off-ramps r are described in Section III-D.

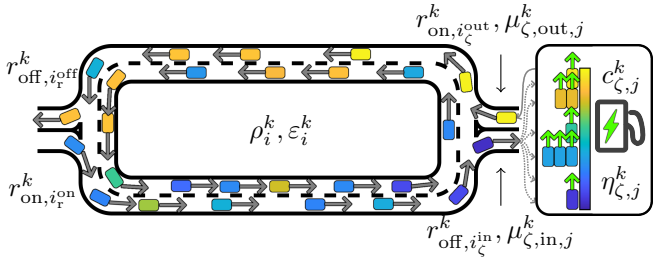

Fig. 3: Discretized CTEC Model illustration. Vehicle SoC is shown colour-coded (colder is lower, warmer is higher), grey arrows represent movement in x on the road (accompanied by a decrease in ε), and green arrows represent change in ε in the charging station (assuming positive charging rate $c_{\zeta,j}^k$).

$$\begin{aligned}q_{i+}^k =& \min\left\{V\overline{\rho}_i^k, \frac{W(P - \underline{\rho}_{i+1}^k) - r_{\text{on},i+1}^k}{1 - \beta_i^k}\right\}, \\ q_{i-}^k =& q_{i-1+}^k(1 - \beta_{i-1}^k) + r_{\text{on},i}^k, \\ \rho_i^{k+1}\varepsilon_i^{k+1} =& \rho_i^k\left(\varepsilon_i^k + d_i^k T\right) + \frac{T}{L}\left(\phi_{i-}^k - \phi_{i+}^k\right),\end{aligned} \tag{18}$$

where $r_{\text{off},i}^k = q_{i+}^k \beta_i^k$ is defined by splitting ratios β_i^k, $\varepsilon_{\text{on},i}^k$ is the average SoC of vehicles entering the road at time step k in cell i, and we need to ensure $r_{\text{on},i}^k \le W(P - \underline{\rho}_i^k)$. Additionally, when calculating $\phi_{i\pm}^k$ in (18), we incorporate the effect of on- and off-ramps by modifying

$$\begin{aligned}\tilde{\rho}_{i-}^k =& \frac{q_{i-}^k}{V}, \qquad \tilde{\rho}_{i+}^k = P - \frac{P - \underline{\rho}_{i+1}^k - \frac{r_{\text{on},i+1}^k}{W}}{1 - \beta_i^k}, \\ \tilde{\varepsilon}_{i-}^k =& \frac{q_{i-1+}^k(1 - \beta_{i-1}^k)\varepsilon_{i-1}^k - r_{\text{on},i}^k \varepsilon_{\text{on},i}^k}{q_{i-}^k},\end{aligned}$$

in (14) and (15), as well as updating $\tilde{v}_{i\pm}^k$, $\tilde{d}_{i\pm}^k$, and $\tilde{\lambda}_{i_\pm^-}^k$ accordingly. Similarly, the charging station dynamics become

$$\begin{aligned}\eta_{\zeta,j}^{k+1} =& \eta_{\zeta,j}^k + \frac{T}{S}\left(\underline{c}_{\zeta,j-1}^k \eta_{\zeta,j-1}^k - \left|c_{\zeta,j}^k\right|\eta_{\zeta,j}^k - \overline{c}_{\zeta,j+1}^k \eta_{\zeta,j+1}^k\right) \\ &+ T\left(\mu_{\text{in},\zeta,j}^k - \mu_{\text{out},\zeta,j}^k\right),\end{aligned} \tag{19}$$

where $\mu_{\text{in},\zeta,j}^k$ and $\mu_{\text{out},\zeta,j}^k$ represent the flows of vehicles with discrete SoC j entering and leaving the charging station, respectively. The flows between the road and the charging station ζ are

$$r_{\text{on},i_\zeta^{\text{out}}}^k = \sum_{j=1}^{N_\varepsilon} \mu_{\text{out},\zeta,j}^k, \quad r_{\text{on},i_\zeta^{\text{out}}}^k \varepsilon_{\text{on},i_\zeta^{\text{out}}}^k = \sum_{j=1}^{N_\varepsilon} \mu_{\text{out},\zeta,j}^k (j-1)S,$$

$$\mu_{\text{in},\zeta,j}^k = \begin{cases}\left(j - \frac{\varepsilon_{i_\zeta^{\text{in}}}^k}{S}\right) r_{\text{off},i_\zeta^{\text{in}}}^k, & j - 1 \le \frac{\varepsilon_{i_\zeta^{\text{in}}}^k}{S} < j, \\ \left(\frac{\varepsilon_{i_\zeta^{\text{in}}}^k}{S} - j + 2\right) r_{\text{off},i_\zeta^{\text{in}}}^k, & j - 2 \le \frac{\varepsilon_{i_\zeta^{\text{in}}}^k}{S} < j - 1, \\ 0, & \text{otherwise},\end{cases}$$

$$\mu_{\text{out},\zeta,j}^k \in \left[0, \left(\frac{1}{T} - \frac{\left|c_{\zeta,j}^k\right|}{S}\right)\eta_{\zeta,j}^k + \frac{\underline{c}_{\zeta,j-1}^k}{S}\eta_{\zeta,j-1}^k - \frac{\overline{c}_{\zeta,j+1}^k}{S}\eta_{\zeta,j+1}^k\right],$$

ensuring both the vehicles and the energy are conserved,

$$r^k_{\mathrm{off},i^{\mathrm{in}}_\zeta}=\sum_{j=1}^{N_\varepsilon}\mu^k_{\mathrm{in},\zeta,j},\quad r^k_{\mathrm{off},i^{\mathrm{in}}_\zeta}\varepsilon^k_{i^{\mathrm{in}}_\zeta}=\sum_{j=1}^{N_\varepsilon}\mu^k_{\mathrm{in},\zeta,j}(j-1)S.$$

The vehicles enter the charging station from cell i^{in}_ζ, and return to the road in cell i^{out}_ζ, typically with $i^{\mathrm{out}}_\zeta = i^{\mathrm{in}}_\zeta + 1$, to ensure that the vehicles return to the road downstream of the point where they left it. The splitting ratios and the flow exiting the charging stations can either be defined according to some heuristics, or used as control inputs.

Note that it is possible to closely approximate (18) by

$$\begin{aligned}\rho^{k+1}_i\varepsilon^{k+1}_i = \rho^k_i\left(\varepsilon^k_i + d^k_{i+}T\right) + \frac{T}{L}\Big((q^k_{i-} - r^k_{\mathrm{on},i})\left(\varepsilon^k_{i-1} + d^k_{i-1+}T\right)\\ + r^k_{\mathrm{on},i}\varepsilon^k_{\mathrm{on},i} - q^k_{i+}\left(\varepsilon^k_i + d^k_{i+}T\right)\Big),\end{aligned}$$

essentially assuming that all vehicles in cell i move at the same constant speed v^k_{i+} during the time step k, with

$$v^k_{i+} = \frac{q^k_{i+}}{\rho^k_i}, \quad d^k_{i+} = \mathcal{D}\left(\mathcal{V}^{-1}\left(v^k_{i+}\right)\right).$$

IV. Control

We exemplify the use of the proposed CTEC model on a regulation problem with tiered priorities, considering a ring road with one charging station and one on-off-ramp pair. The ring road flow is implemented by replacing cell index 0 with N_x and cell index $N_x + 1$ with 1 in all expressions. The studied control goals, in order of priority, are to

1) Ensure that the average SoC $\varepsilon^k_{\mathrm{avg}}$ on the road does not go below $\varepsilon_{\min}$,
2) Minimize the maximum number of concurrent vehicles at the charging station $\eta^{\max}_{\zeta,\mathrm{tot}}$,
3) Regulate the average SoC $\varepsilon^k_{\mathrm{avg}}$ to its reference $\varepsilon_{\mathrm{ref}}$.

A. Control structure

In this work, we assume that we exert no direct control over the charging station dynamics, but instead, the only used control input u^k_β is the ratio of the mainstream flow that leaves the road and enters the charging station,

$$u^k_\beta = \beta^k_{i^{\mathrm{in}}_\zeta} \in [0, 1].$$

All non-full-battery vehicles charge at maximum rate,

$$c^k_{\zeta,j} = \begin{cases} C, & j < N_\varepsilon, \\ 0, & j = N_\varepsilon. \end{cases}$$

and leave with full battery as soon as there is some capacity available on the road,

$$\mu^k_{\mathrm{out},\zeta,j} = \begin{cases} \dfrac{W(P-\underline{\rho}^k_{i^{\mathrm{out}}_\zeta})\tilde{\mu}^k_{\mathrm{out},\zeta}}{V\overline{\rho}^k_{i^{\mathrm{out}}_\zeta-1}\left(1-\beta^k_{i^{\mathrm{out}}_\zeta-1}\right)+\tilde{\mu}^k_{\mathrm{out},\zeta}}, & j = N_\varepsilon, \\ 0, & j < N_\varepsilon, \end{cases}$$

$$\tilde{\mu}^k_{\mathrm{out},\zeta} = \min\left\{\frac{n^k_{\zeta,N_\varepsilon}}{T} + \frac{Cn^k_{\zeta,N_\varepsilon-1}}{S}, r^{\max}_{\mathrm{on},i^{\mathrm{out}}_\zeta}\right\},$$

yielding $r^k_{\mathrm{on},i^{\mathrm{out}}_\zeta} = \mu^k_{\mathrm{out},\zeta,N_\varepsilon}$, and $\varepsilon^k_{\mathrm{on},i^{\mathrm{out}}_\zeta} = 1$. Here, $r^{\max}_{\mathrm{on},i^{\mathrm{out}}_\zeta}$ is the on-ramp capacity, and the road capacity is allocated between the mainstream and the on-ramp flow proportionally to the demand.

We assume that the current total number of vehicles on the road R^k and total energy contained in them E^k,

$$R^k = \sum_{i=1}^{N_x}\rho^k_i L, \quad E^k = \sum_{i=1}^{N_x}\rho^k_i\varepsilon^k_i L, \quad \varepsilon^k_{\mathrm{avg}} = \frac{E^k}{R^k},$$

can both be measured or estimated, providing the average SoC measurement $\varepsilon^k_{\mathrm{avg}}$. Finally, we also assume that the traffic density at the charging station entrance $\rho^k_{i^{\mathrm{on}}_\zeta}$ can be measured, and that the full time profile of the on-ramp flow $r^k_{\mathrm{on},i^{\mathrm{on}}_{\mathrm{r}}}$, the SoC of entering vehicles $\varepsilon^k_{\mathrm{on},i^{\mathrm{on}}_{\mathrm{r}}}$, and the constant splitting ratio towards the off-ramp $\beta_{i^{\mathrm{off}}_{\mathrm{r}}}$ are all known. The average initial traffic density on the road $\rho^0_{\mathrm{avg}} = R^0/(N_x L)$ is taken so that $r^0_{\mathrm{on},i^{\mathrm{on}}_{\mathrm{r}}} = V\rho^0_{\mathrm{avg}}\beta_{i^{\mathrm{off}}_{\mathrm{r}}}$.

The proposed control law can be split into two layers: the outer control loop, regulating the average SoC by setting the reference for the number of vehicles at the charging station u^k_η, and the inner control loop, regulating the number of vehicles at the charging station $\eta^k_{\zeta,\mathrm{tot}}$ using the splitting ratio towards it u^k_β. The control structure is shown in Fig. 4.

B. Inner control loop

The inner control loop regulates the number of vehicles at the charging station $\eta^k_{\zeta,\mathrm{tot}} = \sum_{j=1}^{N_\varepsilon}\eta^k_{\zeta,j}$ to its reference value u^k_η provided by the outer control loop. The controller is a gain-scheduled PI controller with anti-windup, given by

$$u^k_\beta = \frac{\rho^0_{\mathrm{avg}}}{\overline{\rho}^k_{i^{\mathrm{in}}_\zeta}}\max\left\{0, \min\left\{1, K_{\mathrm{p},\eta}e^k_\eta + K_{\mathrm{i},\eta}I^k_{e_\eta}\right\}\right\},$$

$$e^k_\eta = u^k_\eta - \eta^k_{\zeta,\mathrm{tot}}, \quad I^{k+1}_{e_\eta} = \begin{cases} I^k_{e_\eta} + Te^k_\eta, & 0 < u^k_\beta < 1, \\ \frac{u^k_\eta - K_{\mathrm{p},\eta}e^k_\eta}{K_{\mathrm{i},\eta}}, & u^k_\beta = 0 \vee u^k_\beta = 1. \end{cases}$$

Parameters $K_{\mathrm{p},\eta}$ and $K_{\mathrm{i},\eta}$ are tuned empirically to produce good reference tracking with little overshoot, and the gain-scheduling variable $\rho^0_{\mathrm{avg}}/\overline{\rho}^k_{i^{\mathrm{in}}_\zeta}$ aims to compensate for variations in the flow on the road.

C. Outer control loop

The outer control loop sets the reference for the inner control loop u^k_η, and also consists of a PI controller with anti-windup,

$$u^k_\eta = \max\left\{\underline{u}^k_\eta, \min\left\{\overline{u}^k_\eta, K_{\mathrm{p},\varepsilon}e^k_\varepsilon + K_{\mathrm{i},\varepsilon}I^k_{e_\varepsilon}\right\}\right\}, \quad (20)$$

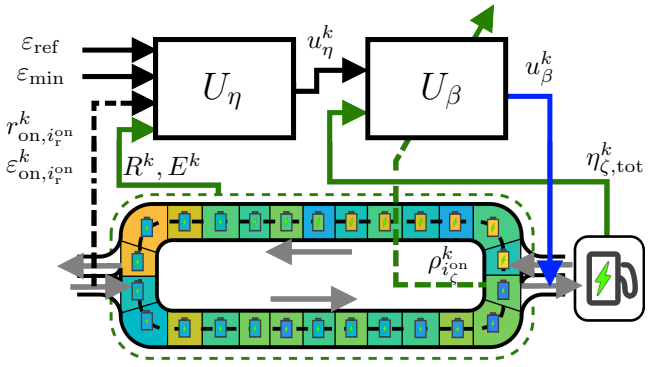

Fig. 4: Full control structure for regulating average SoC, consisting of the outer (U_η) and inner (U_β) control loop.

$$e_\varepsilon^k = \varepsilon_{\mathrm{ref}} - \frac{E^k}{R^k}, \quad I_{e_\varepsilon}^{k+1} = \begin{cases} I_{e_\varepsilon}^k + T e_\varepsilon^k, & \underline{u}_\eta^k < u_\varepsilon^k < \overline{u}_\eta^k, \\ \frac{u_\varepsilon^k - K_{\mathrm{p},\eta} e_\eta^k}{K_{\mathrm{i},\eta}}, & u_\varepsilon^k = \underline{u}_\eta^k \vee u_\varepsilon^k = \overline{u}_\eta^k. \end{cases}$$

The first two control goals can be achieved by tuning parameters $K_{\mathrm{p},\eta}$ and $K_{\mathrm{i},\eta}$, letting $\underline{u}_\eta^k = 0$ and $\overline{u}_\eta^k \to \infty$, or by using these control constraints to address them directly. The two approaches will be compared in simulations.

In the approach using dynamic control constraints, we set $\underline{u}_\eta^k$ to ensure that $\varepsilon_{\mathrm{avg}}^k > \varepsilon_{\min}$, based on a simplified prediction model, and aim to minimize $\eta_{\zeta,\mathrm{tot}}^{\max}$ by setting

$$\overline{u}_\eta^k = \max\left\{ \underline{u}_\eta^k, \max_{h=k-H,\dots,k-1} \eta_{\zeta,\mathrm{tot}}^h \right\}, \tag{21}$$

where H is the time horizon length. The simplified prediction model gives approximate predictions of R^k and E^k for times $h = k+1, \dots, k+H$,

$$\begin{aligned} \hat{R}^{h+1} &= \hat{R}^h + T\left(r_{\mathrm{on},i_{\mathrm{r}}^{\mathrm{on}}}^h - \hat{r}_{\mathrm{off}}^h \right), \\ \hat{r}_{\mathrm{off}}^h &= \begin{cases} \min\{V\sigma, \frac{\beta_{i_{\mathrm{r}}^{\mathrm{off}}}}{1-\beta_{i_{\mathrm{r}}^{\mathrm{off}}}}(V\sigma - r_{\mathrm{on},i_{\mathrm{r}}^{\mathrm{on}}}^h)\}, & R^h > R^0, \\ \min\{r_{\mathrm{on},i_{\mathrm{r}}^{\mathrm{on}}}^h, \frac{\beta_{i_{\mathrm{r}}^{\mathrm{off}}}}{1-\beta_{i_{\mathrm{r}}^{\mathrm{off}}}}(V\sigma - r_{\mathrm{on},i_{\mathrm{r}}^{\mathrm{on}}}^h)\}, & R^h = R^0, \end{cases} \\ \hat{E}_0^{h+1} &= \hat{E}_0^h + T\left(r_{\mathrm{on},i_{\mathrm{r}}^{\mathrm{on}}}^h \varepsilon_{\mathrm{on},i_{\mathrm{r}}^{\mathrm{on}}}^h - \hat{r}_{\mathrm{off}}^h \hat{\varepsilon}_{\mathrm{off}}^h + \hat{R}^h \mathcal{D}(0) \right), \\ \hat{E}^h &= \hat{E}_0^h + \underset{\sim}{u}_\eta^k C(h-k)T, \\ \hat{R}^k &= R^k, \qquad \hat{E}_0^k = E^k, \end{aligned}$$

where we let $\hat{\varepsilon}_{\mathrm{off}}^h = \varepsilon_{\min}$, and the future reference is assumed to be constant, $u_\eta^h = \underset{\sim}{u}_\eta^k$, $h = k+1, \dots, k+H$. Due to the specific form of $\hat{E}^h$, it is straightforward to find the minimum $\underset{\sim}{u}_\eta^k$ for which $\hat{E}^h > \hat{R}^h \varepsilon_{\min}$ for all $h = k+1, \dots, k+H$, which is used as the dynamic control constraint $\underline{u}_\eta^k$,

$$\underline{u}_\eta^k = \max_{h=k+1,\dots,k+H} \frac{\hat{E}_0^h - \hat{R}^h \varepsilon_{\min}}{CT(h-k)}, \tag{22}$$

assuming $E^k > R^k \varepsilon_{\min}$. Finally, PI parameters $K_{\mathrm{p},\eta}$ and $K_{\mathrm{i},\eta}$ are tuned solely to regulate the average SoC, since the first and second control goals are handled by $\underline{u}_\eta^k$ and $\overline{u}_\eta^k$, respectively. Note that the discussed approximate prediction model provides no hard guarantees that the average SoC of the real road will remain within the allowed range, but achieves this goal nonetheless, with suitably tuned PI parameters, as will be shown in simulations.

Symbol	Value	Unit	Symbol	Value	Unit
V	100	km/h	t_{end}	10	h
σ	30	veh/km	ρ_{avg}^0	24	veh/km
P	120	veh/km	$\varepsilon_{\mathrm{ref}}$	0.5	1
L	1	km	$\varepsilon_{\min}$	0.45	1
N_x	50	1	$\varepsilon_{\mathrm{on}}$	0.2	1
C	25	1/h	$r_{\mathrm{on}}^{\mathrm{low}}$	800	veh/h
S	0.1	1	$r_{\mathrm{on}}^{\mathrm{high}}$	1500	veh/h
N_ε	11	1	$t_{\mathrm{start}}^{\mathrm{high}}$	4	h
T	$4 \cdot 10^{-3}$	h	$t_{\mathrm{end}}^{\mathrm{high}}$	5	h
D_0	$-2{\cdot}10^{-2}$	1/h	$\beta_{i_{\mathrm{r}}^{\mathrm{off}}}$	1/3	1
D_1	-10^{-3}	1/km	$i_{\mathrm{r}}^{\mathrm{off}}$	50	1
D_2	$-2{\cdot}10^{-5}$	h/km^2	i_ζ^{out}	25	1

TABLE I: Simulation parameters and their values.

V. Simulation results

The proposed CTEC model and control law are put to the test in a simulation example, whose parameters are given in Table I. The traffic density and SoC on the road are initialized as uniformly distributed random variables

$$\rho_i^0 \sim \mathcal{U}(0, 2\rho_{\mathrm{avg}}^0),\ \varepsilon_i^0 \sim \mathcal{U}(\varepsilon_{\mathrm{ref}} - 0.1, \varepsilon_{\mathrm{ref}} + 0.1),\ i = 1, \dots, N_x,$$

and the charging station is initially empty, $\eta_{\zeta,j}^0 = 0$. Battery discharge rate $\mathcal{D}(\rho)$ is modelled as a polynomial function of traffic speed

$$\mathcal{D}(\rho) = D_0 + D_1 \mathcal{V}(\rho) + D_2 \mathcal{V}(\rho)^2,$$

corresponding to a range of 312.5 km at free flow speed V. The simulation runs from $t = 0$ to $t = t_{\mathrm{end}}$, and the states evolve according to the discretized CTEC model (17)–(19). Vehicles enter the road via the on-ramp in cell 1 at rate

$$r_{\mathrm{on},1}^k = \begin{cases} r_{\mathrm{on}}^{\mathrm{low}}, & t \notin [t_{\mathrm{start}}^{\mathrm{high}}, t_{\mathrm{end}}^{\mathrm{high}}), \\ r_{\mathrm{on}}^{\mathrm{high}}, & t \in [t_{\mathrm{start}}^{\mathrm{high}}, t_{\mathrm{end}}^{\mathrm{high}}), \end{cases}$$

and $\beta_{i_{\mathrm{r}}^{\mathrm{off}}}$ of the flow leaves the road via the on-ramp in cell $i_{\mathrm{r}}^{\mathrm{off}}$. Since the vehicles enter the road via the on-ramp with low SoC $\varepsilon_{\mathrm{on}} < \varepsilon_{\min} < \varepsilon_{\mathrm{ref}}$, the increase in on-ramp flow during $t \in [t_{\mathrm{start}}^{\mathrm{high}}, t_{\mathrm{end}}^{\mathrm{high}})$ acts as a disturbance to the system, causing a drop in the average SoC.

We compared two outer loop PI controller (20) cases:

(a) $K_{\mathrm{p},\varepsilon} = K_{\mathrm{p},\varepsilon}^{(\mathrm{a})}$, $K_{\mathrm{i},\varepsilon} = K_{\mathrm{i},\varepsilon}^{(\mathrm{a})}$, without control constraints, $\underline{u}_\eta^k = 0$, $\overline{u}_\eta^k \to \infty$, and

(b) $K_{\mathrm{p},\varepsilon} = K_{\mathrm{p},\varepsilon}^{(\mathrm{b})}$, $K_{\mathrm{i},\varepsilon} = K_{\mathrm{i},\varepsilon}^{(\mathrm{b})}$, with dynamic control constraints given by (22) and (21),

while the inner loop controller parameters were the same, $K_{\mathrm{p},\eta}$ and $K_{\mathrm{i},\eta}$. Dynamic control constraints were calculated with $H = 500$, corresponding to a time horizon of $HT = 2$ h. The PI parameters are given in Table II. The discrepancy in gain values is due to the fact that $\eta_{\zeta,\mathrm{tot}}$ is in general two orders of magnitude larger than $\varepsilon_{\mathrm{avg}}$ and β.

The simulation results are given in Fig. 5, showing the space-time profiles of ρ and ε, and the SoC-time profile of η for the example simulation run with dynamic control constraints, which are very similar to those without control constraints, and in Fig. 6, showing the average SoC $\varepsilon_{\mathrm{avg}}^k$ and number of charging vehicles $\eta_{\zeta,\mathrm{tot}}^k$ for both cases of control. We can see that both controllers manage to keep the average SoC $\varepsilon_{\mathrm{avg}}^k$ above its minimum allowed value $\varepsilon_{\min}$, and eventually regulate it to $\varepsilon_{\mathrm{ref}}$, but control (a) requires about 18% higher maximum number of charging vehicles than control (b), $\eta_{\zeta,\mathrm{tot}}^{\max,(\mathrm{a})} = 41.746$ compared to $\eta_{\zeta,\mathrm{tot}}^{\max,(\mathrm{b})} = 35.2715$. Since the peak power demand of a charging station grows with the maximum number of concurrent charging vehicles, control law (b) achieves better results by reacting to the disturbance before it arrives, despite using a simplified approximate prediction model.

$K_{\mathrm{p},\eta}$	0.01	$K_{\mathrm{p},\varepsilon}^{(\mathrm{a})}$	100	$K_{\mathrm{p},\varepsilon}^{(\mathrm{b})}$	50
$K_{\mathrm{i},\eta}$	0.1	$K_{\mathrm{i},\varepsilon}^{(\mathrm{a})}$	400	$K_{\mathrm{i},\varepsilon}^{(\mathrm{b})}$	100

TABLE II: Parameters of the PI controllers.

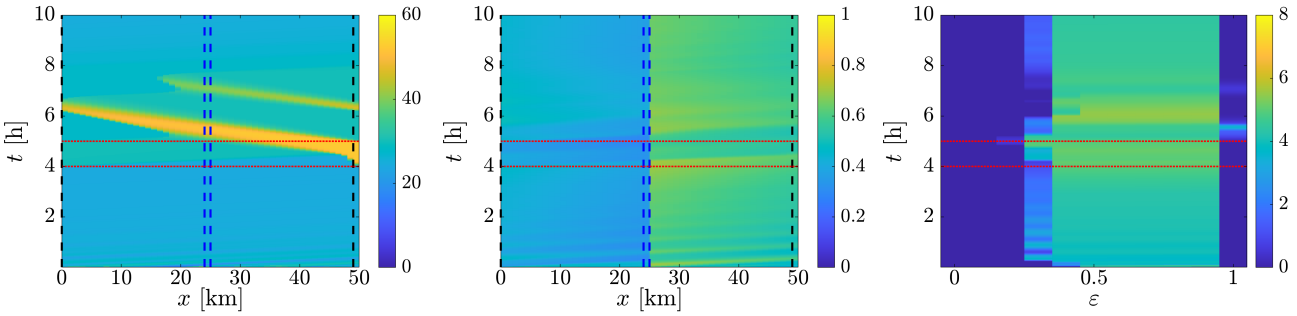

(a) Traffic density profile ρ (b) Traffic SoC profile ε (c) Charging vehicles SoC profile η

Fig. 5: Example simulation results for the case with dynamic control constraints. Disturbance period $[t^{\text{high}}_{\text{start}}, t^{\text{high}}_{\text{end}}]$ is outlined in dotted red, and dashed lines indicate on- and off-ramps (black) and entrance and exit to charging stations (blue).

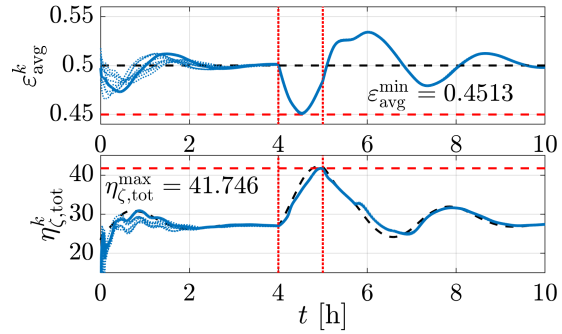

(a) Without control constraints

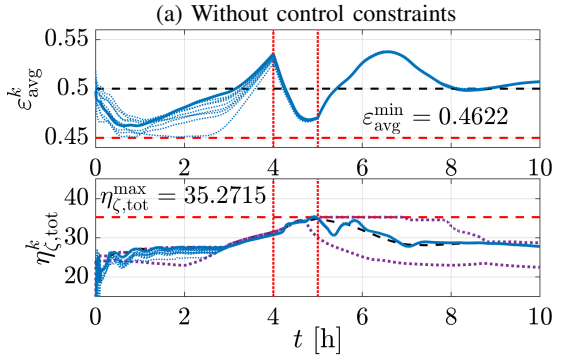

(b) With dynamic control constraints

Fig. 6: Average SoC $\varepsilon^k_{\text{avg}}$ and number of charging vehicles $\eta^k_{\zeta,\text{tot}}$ for the two control cases. Disturbance period $[t^{\text{high}}_{\text{start}}, t^{\text{high}}_{\text{end}}]$ is outlined in dotted red, references ε_{ref} and u^k_η are shown in dashed black, and dynamic control constraints $\underline{u}^k_\eta$ and $\overline{u}^k_\eta$ in dotted purple. Other simulation runs are shown in dotted blue.

VI. Conclusion

In this paper, we attempt to bridge the gap between the transportation and power system by proposing a macroscopic model that captures the coupled flows of EV traffic and the energy, the CTEC model. The model extends the LWR traffic model by adding the advection, discharging, and charging dynamics of the energy contained by EV batteries. The discretized model is used in simulations to design and test a control law with tiered control objectives, first ensuring the average SoC does not go below some value, then minimizing the maximum number of concurrently charging vehicles, and finally regulating the average SoC to its reference value.

Note that the addition of on- and off-ramps were only considered for the discretized model, due to the complications with the Riemann problem that they cause. For future work, the full Riemann problem should be solved in order to be able to handle exactly merges and diverges, including on- and off-ramps, as well as to extend the model from one road to a road network. Furthermore, the simplifying assumption that the traffic consists solely of EVs should be dropped, and the model should be extended to the case when only a portion of vehicles are electric. Finally, once the model is extended to the full network, the power system requirements could be explicitly considered, and control laws using EVs to provide flexibility designed.

Acknowledgements

This project has received funding from the European Research Council (ERC) under the European Union's Horizon 2020 research and innovation programme (grant agreement 694209), http://scalefreeback.eu.

References

[1] European Commission and Directorate-General for Energy, *Effect of electromobility on the power system and the integration of RES : study S13*. Publications Office, 2019.

[2] L. Thibault, G. De Nunzio, and A. Sciarretta, "A unified approach for electric vehicles range maximization via eco-routing, eco-driving, and energy consumption prediction," *IEEE Transactions on Intelligent Vehicles*, vol. 3, no. 4, pp. 463–475, 2018.

[3] M. Alizadeh, H.-T. Wai, M. Chowdhury, A. Goldsmith, A. Scaglione, and T. Javidi, "Optimal pricing to manage electric vehicles in coupled power and transportation networks," *IEEE Transactions on control of network systems*, vol. 4, no. 4, pp. 863–875, 2016.

[4] K. Qian, C. Zhou, M. Allan, and Y. Yuan, "Modeling of load demand due to ev battery charging in distribution systems," *IEEE transactions on power systems*, vol. 26, no. 2, pp. 802–810, 2010.

[5] C. Le Floch, E. C. Kara, and S. Moura, "PDE modeling and control of electric vehicle fleets for ancillary services: A discrete charging case," *IEEE Transactions on Smart Grid*, vol. 9, no. 2, pp. 573–581, 2016.

[6] G. Wenzel, M. Negrete-Pincetic, D. E. Olivares, J. MacDonald, and D. S. Callaway, "Real-time charging strategies for an electric vehicle aggregator to provide ancillary services," *IEEE Transactions on Smart Grid*, vol. 9, no. 5, pp. 5141–5151, 2017.

[7] H. Lund and W. Kempton, "Integration of renewable energy into the transport and electricity sectors through v2g," *Energy policy*, vol. 36, no. 9, pp. 3578–3587, 2008.

[8] Z. Zhou, X. Zhang, Q. Guo, and H. Sun, "Analyzing power and dynamic traffic flows in coupled power and transportation networks," *Renewable and Sustainable Energy Reviews*, vol. 135, p. 110 083, 2021.

[9] C. Fiori, K. Ahn, and H. A. Rakha, "Power-based electric vehicle energy consumption model: Model development and validation," *Applied Energy*, vol. 168, pp. 257–268, 2016.

[10] X. Qi, G. Wu, K. Boriboonsomsin, and M. J. Barth, "Data-driven decomposition analysis and estimation of link-level electric vehicle energy consumption under real-world traffic conditions," *Transportation Research Part D: Transport and Environment*, vol. 64, pp. 36–52, 2018.

[11] J.-P. Lebacque and M. M. Khoshyaran, "A variational formulation for higher order macroscopic traffic flow models of the gsom family," *Procedia-Social and Behavioral Sciences*, vol. 80, pp. 370–394, 2013.

[12] M. J. Lighthill and G. B. Whitham, "On kinematic waves II. a theory of traffic flow on long crowded roads," *Proceedings of the Royal Society of London. Series A. Mathematical and Physical Sciences*, vol. 229, no. 1178, pp. 317–345, 1955.

[13] A. Aw and M. Rascle, "Resurrection of "second order" models of traffic flow," *SIAM journal on applied mathematics*, vol. 60, no. 3, pp. 916–938, 2000.

[14] C. F. Daganzo, "The cell transmission model: A dynamic representation of highway traffic consistent with the hydrodynamic theory," *Transportation Research Part B: Methodological*, vol. 28, no. 4, pp. 269–287, 1994.

[15] J.-P. Lebacque, "The Godunov scheme and what it means for first order traffic flow models," *Proceedings of the 13th International Symposium on Transportation and Traffic Theory*, pp. 647–677, 1996.